AIAA JOURNAL
Vol. 48, No. 10, October 2010

Numerical Simulation on Plasma Circulation Control Airfoil

P. F. Zhang,* B. Yan,† A. B. Liu,‡ and J. J. Wang§
Beijing University of Aeronautics and Astronautics, 100191 Beijing, People's Republic of China

DOI: 10.2514/1.J050133

A novel plasma circulation control technique is proposed to overcome the disadvantage of conventional jet circulation control about the requirement for air source. By employing the plasma actuator on the trailing edge of the airfoil, the plasma-induced wall jet is tangential to the airfoil surface and served as Coanda blowing jet, which makes the trailing-edge detachment point migrate to the lower surface of the airfoil. In this way, the circulation and the lift of airfoil are directly controlled by the plasma actuator. The effectiveness of plasma circulation control on the aerodynamic characteristics improvement of NCCR 1510-7067N airfoil is demonstrated by solving the Reynolds-averaged Navier–Stokes equations. The plasma actuator is modeled with a phenomenological model by adding the body force source terms to the governing equations. The results indicate that the efficiency of plasma circulation control for lift augmentation is superior to that of conventional jet circulation control method. The lift augmentation efficiency after the location optimization reaches $\Delta C_L/C_\mu = 134.86$, which is much higher than the maximum lift augmentation efficiency 80 for conventional jet circulation control. The optimal location for the plasma actuator in plasma circulation control is downstream of the boundary-layer separation point with proper distance, where the plasma actuator makes the separated shear layer reattach to the airfoil surface and delays the trailing-edge stagnation by Coanda effect.

Nomenclature

a	=	height of the plasma region, mm
b	=	width of the plasma region, mm
C_D	=	drag coefficient
C_L	=	lift coefficient
C_P	=	surface pressure coefficient
C_μ	=	jet momentum coefficient
c	=	chord length, m
D_c	=	strength of the plasma actuator
d	=	distance between the electrodes of the plasma actuator, mm
E_b	=	breakdown electric field strength, kV/cm
E_i	=	electric field strength in i direction, kV/cm
e_c	=	charge of electron,
F_i	=	body force in i direction
h	=	slot height, m
U_a	=	applied root mean square voltage, kV
U_∞	=	freestream velocity of incoming flow, m/s
$u_\tau(n)$	=	velocity tangential to airfoil surface, m/s
α	=	angle of attack, deg
ΔC_L	=	lift coefficient augmentation
Δt	=	discharge time of the plasma actuator, μs
δ	=	boundary-layer momentum thickness, m
θ	=	annular angle of the plasma region origination point, deg
ρ_c	=	charge electrons density, $1/\text{cm}^3$
ϑ	=	frequency of applied voltage, khz

Received 12 August 2009; revision received 4 February 2010; accepted for publication 8 June 2010.

*Associate Professor, Institute of Fluid Mechanics, Key Laboratory of Fluid Mechanics (Ministry of Education); pfzhang@buaa.edu.cn.
†Graduate Student, Institute of Fluid Mechanics; yabo_001@hotmail.com.
‡Graduate Student, Institute of Fluid Mechanics; liuibing@gmail.com.
§Professor, Institute of Fluid Mechanics; jjwang@buaa.edu.cn. Member AIAA.

I. Introduction

CIRCULATION control (CC) concept is inspired by the well known Coanda effect, invented by Romanian inventor Henri Coanda in early 1930s [1]. It means the tendency of fluids to adhere to curved surfaces even for surfaces that are highly curved. As long as the equilibrium between the centrifugal forces and the pressure gradient exists, the fluid remains attached to the surface and no separation occurs. It is actually a well known phenomenon which can be seen even when pouring water from a round edged container.

Conventional airfoils have a sharp trailing edge in general. The Kutta condition will be readily satisfied for this kind of airfoil, and determines the circulation over the airfoil at a given freestream condition and angle of attack. The CC airfoil takes advantage of Coanda effect by blowing a small, high-velocity jet over a highly curved surface, such as a rounded trailing edge. Since the airfoil trailing edge is not sharp, the Kutta condition is not fixed and the trailing-edge detachment point is free to move along the surface (as shown in Fig. 1a). With blowing, the trailing-edge detachment point moves toward the pressure side of the foil, thus changing the circulation of the entire airfoil and increasing lift. Since the jet mass flow rate is readily controlled, this results in direct control of the separation point location, and thus the circulation and lift, as suggested by the name of this concept [2].

CC technology has been widely investigated over the past 25 years [3]. It provides simplification of actuation, reduction in weight and number of moving parts as compared with conventional high-lift systems, which contribute to noise, add to the weight of the aircraft, and are costly to build and maintain.

The early research work about CC was done in England, which was desired to produce a stoppable-rotor vertical tack-off and landing (VTOL) aircraft. In this concept, a blown two-bladed rotor could produce very high-lift per blade to make the aircraft hover, then be stopped and stowed within the helicopter fuselage for forward fixed-wing flight. A circular-cylinder cross section slotted-pipe rotor appeared to be an ideal solution [4]. After 1970, this concept was pursued in the United States by Navy researchers. The David Taylor Naval Ship Research and Development Center (DTNSRDC) became a major center for CC research, where the approach taken was to develop lower-drag, high-lift rotor blade sections by converting the circular-cylinder profile into a much thinner blown elliptic airfoil. The obtainable lift coefficient C_L of such single-slotted CC rotor elliptic airfoil is lower than that of previous cylindrical airfoil, but the required jet momentum coefficient C_μ is a factor of 10–20 less, which yields the very high force augmentation efficiency, $\Delta C_L/C_\mu$

of 80, representing an 8000% return on the momentum invested [5,6].

The original designs of CC airfoils, such as elliptic airfoil, usually had large radius rounded trailing edges to maximize the lift benefit, since the small radius CC airfoils with larger slot height could caused jet detachment and sudden lift loss at higher momentum coefficient. However, these designs also produced very high drag [7]. In particular, the high drag associated with the blunt, large radius trailing edge can be prohibitive under cruise conditions when CC is no longer necessary.

There were two ways to reduce the drag associated with the large radius trailing edge. The first one was a fixed simple radius reduction, and the other was the advanced circulation control wing (CCW) flap, i.e., a circulation hinged flap. From the nondeflectable standpoint [8], a supercritical-type airfoil was employed as the baseline because it already had a bluff base thickness. With this configuration, the no-moving-parts CC airfoils generate the same or greater lift as the maximum C_L of a triple-slotted-flap airfoil with mechanical slat, meanwhile, with very slight blowing it can reduce C_D to less than the baseline supercritical airfoil, while increasing lift as well. The second approach to the drag problem was a simple CCW flap with a curved upper surface and a sharp trailing edge [6,9]. The upper surface of the CCW flap is a second much larger radius arc. The flap can be deflected from 0 to 90 deg. During takeoff or landing, the flap is deflected. Then this large radius on the upper surface produces a large jet turning angle, leading to a high-lift. While in cruise, the flap is retracted and the transformed airfoil has a conventional sharp trailing-edge shape results, which greatly reduces the drag of airfoil. This kind of flap does have some moving elements, which increase the weight and complexity over the earlier CC airfoil design shown in Fig. 1a. But overall, the hinged flap design still maintains most advantages of CC airfoil, such as high-lift, while greatly reducing the drag in cruising condition associated with the rounded trailing edge.

NASA Langley Research Center (LaRC) also has done the studies to evaluate the effectiveness of applying the advanced CCW to an advanced subsonic transport [9,10]. The typical 15 moving elements per wing of Boeing737 commercial aircraft were replaced with the CCW single element flaps and leading-edge blowing, yielding perhaps a maximum of three components per wing. Using only fan bleed air, replacing the conventional flaps with CCW, was able to triple the usable lift at takeoff and produce the ground roll reductions. These pneumatic benefits are not limited to subsonic transports. Englar et al. [11] also applied CCW to a generic high-speed civil transport configuration developed by Georgia Tech Research Institute for NASA LaRC. By employing simplified CCW flaps, the effectiveness of combined pneumatic high-lift devices and control surfaces on the HSCT aircraft to reduce takeoff wing area or approach angle was confirmed.

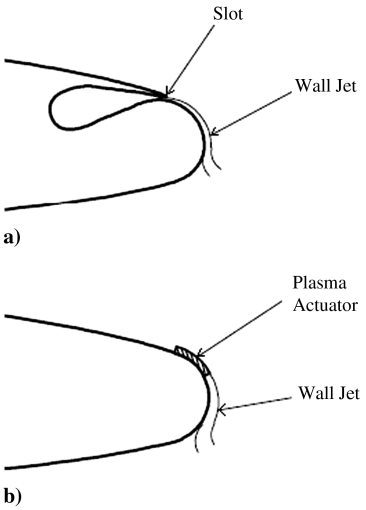

Fig. 1 Sketch for the jet CC airfoil (upper) and the PCC airfoil (lower).

The CC technique does not pertain solely to aeronautical engineering. Other fields include submarine control surfaces (lift at low speeds), boundary-layer control on highly deflected flaps, helicopters rotors without collective and cyclic pitch controls, drag reduction on trucks, thrust vectoring, and turbine blades cooling. More detail applications about CC have been described in the review paper by Englar [3].

CC by Coanda blowing over a rounded trailing edge has been extensively investigated for over 25 years and is by far the most blowing power efficient method for high-lift generation. However, one of the significant penalties associated with CC systems is the power required to supply the blowing air source [3]. Another part of this problem is that the CC mass flow required per pound of aircraft, and therefore the pneumatic power required, is proportional to the square of the takeoff velocity [3,12]. In the past 25 years, only two CC aircrafts have ever been build and flight-tested, which were the West Virginia University (WVU) CC Technology Demonstrator Short Takeoff/Landing (STOL) aircraft flight-tested in 1974 and the Grumman A-6A flight-tested in 1979 [12]. With CC, the WVU CC Technology Demonstrator required all the available 180 HP propeller thrust during fly at slow speed and high C_L, which means flying on the backside of the power curve. This leaves no power to spare to assist in wing stall recovery. So John [12] argued that this can explain why no more than two such airplanes have been build in the past long times.

Different from traditional blowing method, the plasma actuator generates a body force on the fluids tangential to the surface in the downstream direction, which induces a wall blowing jet without requirement for air source and pneumatic system. In present study, a novel plasma circulation control (PCC) concept is proposed to overcome the disadvantage of conventional jet CC method. The plasma actuator is fully electronic with no moving parts, extremely fast response, very low mass, low input power, and easy to simulate their effect in numerical flow solvers [13]. In particular, it is flexible, so it can be formed to various shapes and located on air vehicles with relative ease. There are no other known actuators that have such flexibility [14], which is a unique advantage for plasma actuator used as CC device. In CC, the Coanda blowing jet is essentially required to be tangential to the surface, which makes the blowing jet adhere to the curve wall matching the Coanda effect condition. In jet CC, the slot for the conventional pneumatic system should be placed at the location with large radius to let the jet tangential to the airplane surface. Otherwise, it should be specially designed. With the flexibility and the induced wall jet tangential to the air vehicles surface anywhere, the plasma actuator can be placed at any complex sharp surfaces of the airplane, and it is easy for the PCC device to be integrated to the existing aircraft with little modification.

The plasma actuator considered here is based on surface dielectric-barrier discharge (DBD). This new discharge method was invented by Roth and protected by a U.S. patent since 1995 [15]. This surface plasma has considerably influenced the research on airflow control because its simplicity allowed many researchers in aerodynamics to work on this subject, without necessarily being a specialist in plasma physics [16]. The single DBD plasma actuator consists of two electrodes, one exposed to the air and the other covered by dielectric material. Velocity measurements indicate that the primary result of the averaged plasma-induced flow is the formation of a wall jet which imparts momentum to the fluid [13]. In present study, a plasma actuator is attached to the blunt trailing edge of an elliptic airfoil, which induces the blowing jet tangential to the surface and used as the Coanda blowing jet (as seen in Fig. 1b). The effect of the PCC to increase the airfoil lift is examined by numerical simulation, and the influence of plasma actuator location is also studied.

II. Governing Equations and Numerical Method

In present work, the plasma actuator is simulated with a phenomenological model proposed by Shyy et al. [17] which adds the body force source to the conservation equations for momentum and energy representing the plasma effect. The method provides the primary control mechanism introduced by the plasma actuator

which, as described earlier, consists of momentum injection yielding a wall jet. Of course it is not perfect to handle the interaction of ionized particles of plasma with neutral gas, but can capture the key features of plasma structure [18], such as momentum generation, in higher pressure discharges, which can be assumed to be close to equilibrium plasma [19]. The most advantage of this model is computationally inexpensive, which makes it is attractive for probing various new flow applications in preliminary. Now it becomes the most widely used plasma model in literatures for plasma actuation flow control simulation.

For example, Gaitonde et al. adopted this phenomenological approach to modeling plasma-based separation control in a NACA 0015 airfoil wing section [20]. Jayaraman and Shyy [21] employed it to investigate aerodynamics and thermal management issues. Orlov [22] and He and Corke [23] used the linear body approach along with a lumped element circuit model to study leading-edge separation and flow control over a hump, respectively. Visbal and Gaitonde [24] explored the potential of the plasma actuator in the control of turbulent and transitional separated flows with this model. Rizzetta and Visbal [25] employed the phenomenological body force approach to model the plasma-based separation control for a transitional highly-loaded turbine blade at a Reynolds number about 25,000. Vo [26] and Lemire et al. [27] used the body force approach to study the control of rotating stall in axial compressors by plasma actuation. Fu et al. [28] used this model to simulate the separation flow control on NACA 0015 airfoil, and got good agreement of numerical and experimental results. It can be seen the phenomenological model used in present study is widely used in numerical investigation to explore the new application of plasma flow control as a testbed. Gaitonde et al. [29] compared the phenomenological model with a first-principles approach, and demonstrated that the same qualitative flow control behavior is captured with both methods.

In present simulation, the flow field is assumed to be described by the Reynolds-averaged Navier–Stokes (RANS) equations, augmented by source terms representing the local forcing of the SDBD device [21]. For steady incompressible flow, the conservation of mass and momentum equations can be written as

$$\frac{\partial u_i}{\partial x_i} = 0 \qquad \rho \frac{\partial (u_i u_j)}{\partial x_j} + \frac{\partial p}{\partial x_i} = \frac{\partial \tau_{jj}}{\partial x_j} + F_i \tag{1}$$

In the momentum equation, the body force introduced by the plasma actuator is given by

$$F_i = \vartheta \alpha \rho_c e_c \Delta t E_i \delta \tag{2}$$

where ϑ is the frequency of the applied voltage, α is a factor to account for the collision efficiency, ρ_c is the electron number density, e_c is the charge of electron, Δt (during which the plasma is formed) corresponds to one half cycle, E_i is the electric field strength in i direction, and δ is the Dirac delta function of space. The Dirac delta function means that the body force acts only in the regions where the plasma is present [17]. To ensure this restriction, the delta function is written as

$$\delta = \begin{cases} 1 & E > E_{\text{cr}} \\ 0 & E \le E_{\text{cr}} \end{cases} \tag{3}$$

All the computations presented here were carried out using the segregated solver in the Fluent code. A steady form of RANS equations was used as the governing equations. The PISO algorithm was used to generate steady-state solutions. The advective terms were discretized using the second-order upwinding, and the viscous terms using second-order central differencing scheme. First order upwinding was used on the turbulent kinetic, turbulent dissipation rate and Reynolds stress equations. The high-order terms were treated using a deferred correction approach. The discretized algebraic equations were solved using a pointwise Gauss–Seidel iterative algorithm. For this segregated solver, the convergence criteria used was to require the normalized residual to be less than 10^{-6} for the energy equation and less than 10^{-5} for all other equations.

Because of the complexity of the flow structures around the CC airfoil, which includes a wall jet with convex mean streamlines and its diffusion into a coflowing wake flow, turbulence modeling plays an important role in the success of such simulations. Liu et al. [30] reported good results from numerical solutions for CC airfoils using algebraic and Spalart–Allmaras (SA) one-equation eddy-viscosity turbulence models. However, Chang et al. [31] and Slomski et al. [32] indicated that the CC for the airfoils used in Liu et al. simulation [30] was essentially a blown flap method, where the jet separated from a sharp, rather than bluff, trailing edge, which fixes the separation point. The general CC airfoil problem requires the jet to separate at some point along a curved wall (the bluff trailing edge), so the turbulence model used in the simulation is a critical factor for the correct prediction. Slomski et al. [32] also showed that the k-ε and realizable k-ε models was able to reasonably predict the lift generated by the CC for lower rate of blowing jet. However, at higher blowing rate, only the Reynolds stress model (RSM) continues to capture the physics of the CC problem and hence reasonable lift prediction. Paterson and Baker [33] used incompressible Reynolds-averaged Navier–Stokes and detached eddy simulation methods to study the flow characteristics of three-dimensional CC foil. They demonstrated that a linear Reynolds-stress closure and a blended k-ω/k-ε turbulence model was able to successfully predict the pressure distribution trends with large jet momentum coefficient, which is contrary to Slomski et al. conclusions [32]. They stated that higher-order curvature-corrected models may only be required to resolve localized details such as the maximum suction peak on the Coanda surface. Swanson et al. [34] investigated the use of different turbulence models on flows around CC airfoil. The tested turbulence models include the one-equation SA model, the SA model with curvature correction (SARC), the two-equation shear-stress transport model (SST), and the two-equation model for the turbulent kinetic energy and enstrophy k-ζ. At the low jet momentum coefficient, the k-ζ model performed similar to the SARC model, whereas the SA and SST models produced significantly greater delay in separation. Among the models tested, only the SARC model produced physically realistic solutions at the highest blowing rate. Recently, Salem and Ragab [35] compared the influence of different turbulence models which were used to simulate the subsonic flow field around the Coanda disc model with omnidirectional blowing. Whereas only RSM produced physically plausible flow, other models such as k-ε or SA model (without streamline curvature correction) failed to produce physically meaningful results. As indicated by Swanson and Rumsey [36], the traditional turbulence models sometimes work and sometimes do not, and computational solutions tend to be highly sensitive to numerical parameters and methods of solution. In present study, the full Reynolds stress model (FRSM), which is robust to handle general aerodynamic flows of CC airfoil, is chosen to simulate the flow characteristics of airfoil with PCC, and full validation about the numerical method to simulate the jet CC control airfoil flow is done.

III. Geometry Modeling and Grid Generation

The airfoil that is now to be tested is called NCCR 1510-7067N, which has been wind tunnel tested at DTNSRDC by Abramson in 1977 [37], which was chosen as the benchmark case for numerical validation about jet CC at the 2004 NASA/Office of Naval Research CC Workshop [38]. Except for the plenty experimental data of force and pressure [37], there are numerous articles [31,32,39] published to simulate the flow around this airfoil, which is convenient for present work to compare with. The airfoil has an elliptic section with 15% thickness to chord ratio, 1% camber. The slot is located on the upper surface at $x/c = 96.7\%$ and the slot height to chord ratio h/c is 0.003. More detail about the airfoil and slot configuration can be seen in Fig. 2a. To set the plasma actuator at the airfoil trailing edge, the original trailing edge with slot is replaced by a circular arc, which is smoothly connected with the main part of the airfoil. Figure 2b shows the trailing-edge details of the original airfoil and the modified one. The dashed line is the original NCCR 1510-7067N airfoil trailing edge, which has a slot at the airfoil upper surface to supply air for jet CC. The continuous line represents the shaped one used in present

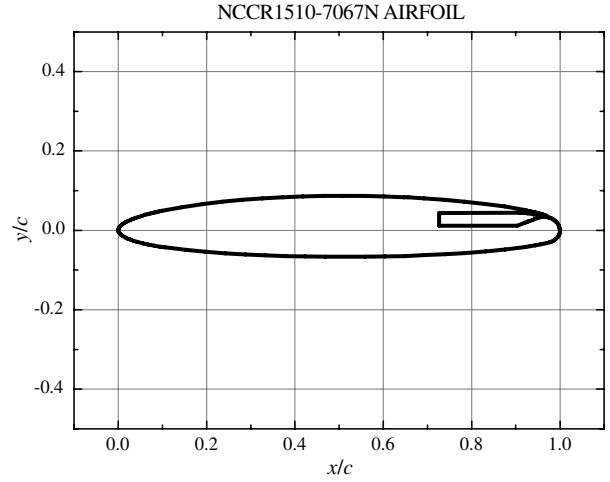

a) NCCR 1510-7607N airfoil

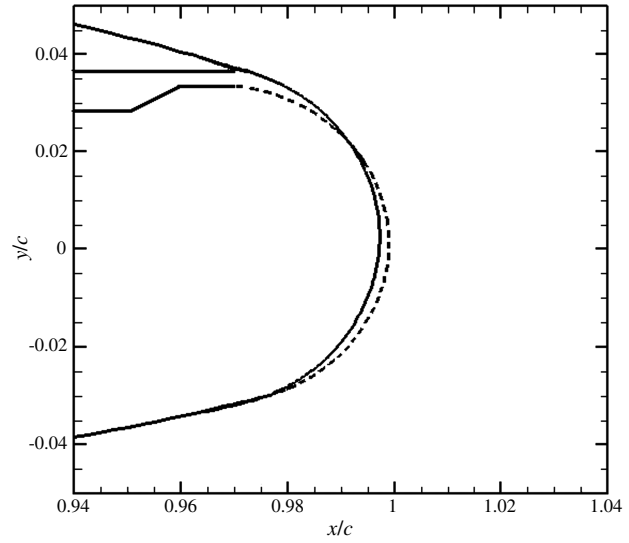

b) Modification of the trailing edge curve

Fig. 2 Airfoil in simulation and the trailing-edge modification.

simulation, which has smooth transient curve for the trailing edge for the plasma actuator to be set. The airfoil chord length in PCC simulation is $c = 1$ m, and the freestream velocity of incoming flow U_∞ is 10 m/s, which yields the Reynolds number based on the airfoil chord length is 6.84×10^5.

A delta shape region with electric field induced by the plasma actuator is assumed to adhere to the airfoil trailing edge, with the height $a = 1.5$ mm and the width $b = 3$ mm. With plasma actuator on, the ambient neutral air is absorbed into the plasma region and forms a wall jet, which is tangential to the surface of airfoil trailing edge and serves as Coanda blowing jet (as shown in Fig. 1b). The plasma actuator parameters adopted in present study refer to those in Shyy et al.'s investigation [17], which used a typical SDBD plasma actuator configuration as in previous experimental study [40,41]. The various parameters here are, the frequency of applied voltage $\vartheta = 3$ kHz, the charge electrons density $\rho_c = 1.03 \times 10^{11}/\text{cm}^3$, the applied voltage $U_a = 10$ kV rms, the breakdown electric field strength $E_b = 30$ kV/cm, the discharge time $\Delta t = 67$ μs and the distance between the electrodes $d = 0.25$ mm. The details about the plasma actuator parameters can refer to Shyy et al.'s simulation [17] and Roth et al.'s experiments [40,41]. More details about the electric field distribution and the body force calculation can be seen in Shyy et al.'s paper [17]. As mentioned above, the Reynolds number of the flow around the airfoil is 6.84×10^5. The velocity of the freestream over the airfoil of chord 1 m is 10 m/s. The convection time scale under this condition (chord length/freestream velocity) is $\mathcal{O}(0.1$ s). Compared with the plasma operating frequency-based (kHz) time scale ($\mathcal{O}(10^{-4})$ s) and the species convection/reaction time scale ($\mathcal{O}(10^{-9})$) [18], it is clear that the flow time scale being separation over roughly three orders of magnitude. So the plasma actuator can be treated as a steady body force distribution in present study under this Reynolds number.

To scale the strength of the plasma actuator, a nondimensional parameter D_c is adopted to represent the ratio of the electrical force to the inertial force [21]. It is given by

$$D_c = \frac{q_c E_0 L}{\rho U_\infty^2} \tag{4}$$

Here, q_c is the charge density and can be calculated as $\rho_c \cdot e_c$, thus the strength of plasma actuator D_c in present study is 22.7. The maximum velocity of plasma-induced wall jet in this configuration is about 30 m/s, as to say the Mach number is less than 0.1. So the flow is absolutely incompressible flow.

All of the computations are performed using an orthogonal C-grid topology as shown in Fig. 3a. The top and bottom far field boundaries are ten chord lengths from the airfoil. The upstream velocity inlet boundary is nine chord lengths away from the airfoil leading edge, and the downstream outflow boundary is 20 chord lengths away. The grid is constructed using the grid generation code Gridgen. The algebraic stretching function of TANH is used to determine the circumferential and normal point distribution of the airfoil surface. To examine the effect of grid resolution on the aerodynamic forces, three structured two-dimensional grid systems, i.e., the coarse, the medium and the fine cases, with grid points of 300×100, 400×150 and 600×200 respectively, are adopted. It is observed that the aerodynamic forces calculated with the medium grid and fine grid almost have no difference, but the suction peaks near the leading and trailing edges of airfoil with the coarse grid are a little smaller than those with the former two grid systems. So the medium grid is proper for present study and is used in the following simulations. For the circumferential 400 grid points, there are 250 grid points placed at the

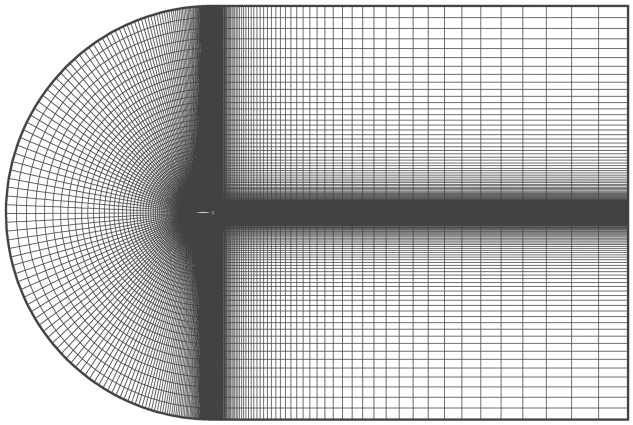

a) Grid distribution around the airfoil

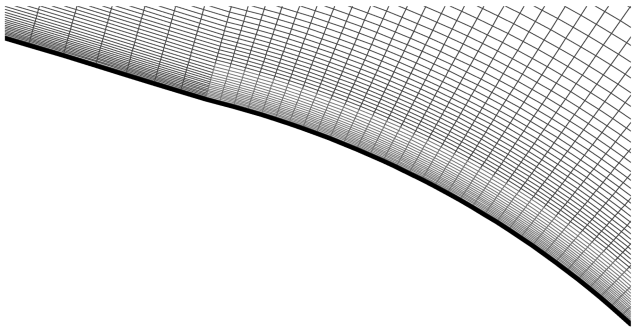

b) Details of grid in the vicinity of trailing edge, including the plasma region

Fig. 3 C-type grid topology and the refined grid near the trailing edge.

upper and lower surface of the airfoil, and the rest are placed in the wake region.

Figure 3b shows a closer view of the grid in the vicinity of the airfoil trailing edge. The plasma region adhered to the airfoil trailing edge is also included with different color. To add the body force source terms to the momentum equation in this region, the annular arc region with height $a = 1.5$ mm is defined as a separated control volume in Fluent, and the body force source is added to the governing equations in this region by user-defined function incorporated in Fluent code. Grid clustering is evident near the surface of the airfoil, as well as near the trailing edge, to obtain reasonable resolution of the boundary layer and the plasma region. The first grid point above the surface is located at $y^+ \approx 1$, and the grid points in the plasma region is 150×30, which is adequate to capture the flow structures induced by the plasma [42].

IV. Numerical Method Validation

The validation of numerical method used in present study to simulate the plasma actuator induced flow has been done by Shyy et al. [17] The predicted velocity profiles at different upstream and downstream locations match well with the experimental results. They also gave the effects of incoming flow velocity and the applied voltage frequency on the magnitude of the maximum wall jet velocity induced by the plasma actuator. The results also had good agreement with theoretical analysis. Jayaraman et al. [43] predicted the correlation of body force with applied voltage with a dependence of $V^{3.0}$, which is quite close to the dependence from the experiments of Van Dyken et al. [44]. Grundmann et al. [45] also used this phenomenological model to flow field induced by a single asymmetrical arranged plasma actuator, and they also done experiment for validation. The correlations of induced maximum velocity with applied voltage fitted quite well with the experimental results, which presents the same power low of $V^{3.5}$ relation with that of Corke and Matlis [46]. The simulated momentum flow rate also agreed well with the experimental results. All these comparisons indicates that the phenomenological mode used in present study is adequate to capture the fluid dynamic characteristics of plasma actuator, hence it is no doubt that the basic feature of CC on the airfoil by plasma actuator can be well investigated by this model.

In present study, we just validate the accuracy of numerical method to predict the aerodynamic characteristics of NCCR 1510-7067N airfoil with jet CC. The predicted lift coefficient vs the jet momentum blowing coefficient C_μ of airfoil at zero angle of attack is plotted in Fig. 4, which also contains the benchmark experimental data [37] and the numerical simulated data by Chang et al. [31], Slomski et al. [32], and Messam [39]. For the validation case, the chord length of the airfoil is $c = 8$ inch, that is to say 0.2032 m. The incoming flow velocity is 41.65 m/s, and the Reynolds number based on the airfoil chord length is 5.8×10^5. Without jet CC ($C_\mu = 0$), the lift coefficient of NCCR 1510-7067N airfoil obtained by present study matches well with the previous experimental and numerical results. With Coanda blowing jet, the trend of lift coefficient varies with the jet momentum blowing coefficient is similar to that in the experiment, and the predicted curve falls in the divergence band of experimental and previous numerical data.

To further validate the numerical method accuracy, the flow structure and the pressure distribution of airfoil with jet CC at $C_\mu = 0.092$ are given in Figs. 5 and 6, respectively. At this blowing rate, the jet remains attached to the trailing-edge Coanda surface, and the trailing-edge detachment point is pushed aft and thus close to the lower surface of airfoil. The simulated flow field closely agrees with that of Chang et al. [31] simulated by FRSM (Fig. 5a), which is the physically plausible flow. The predicted pressure distribution also consists to Abramson's experimental results [37], especially the suction peak near the trailing edge, which means the Coanda blowing jet near the trailing edge is right captured by present numerical method. With these comparisons, the conclusion can be drawn that the numerical method used in present study is accurate to simulate the flow of CC airfoil, both in aerodynamic force prediction and flow structure simulation.

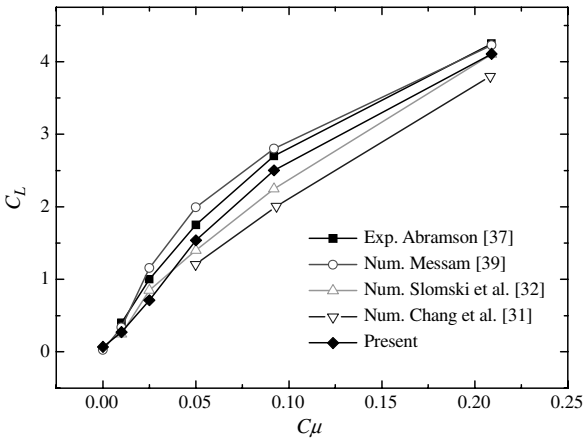

Fig. 4 Comparison of lift coefficients of NCCR 1510-7067N airfoil with jet CC obtained in present simulation with previous studies.

V. Plasma Circulation Control

In this section, the plasma actuator is placed at NCCR 1510-7067N airfoil trailing edge, and is originated from the point, at which the Coanda trailing edge is connected with the airfoil upper surface, and is right at the same chord location of the jet slot of the original airfoil (Point A shown in Fig. 7). The control volume for body source addition, which represents the plasma region in simulation, is an annular sector close attached to the trailing edge with the circumferential length and radial height of 3 mm and 1.5 mm, respectively. In engineering application, this plasma actuator with totally close adhering to the wall can be fabricated with flexible materials for printed circuit board, such as Kapton and Telflon [14]. For the convenient description in following parts, the Cartesian coordinate system in this paper is defined as these: the x-axis is parallel to the chord of the airfoil, the y-axis is perpendicular to the x-axis and the origin O is at the leading edge of airfoil. For the location of the plasma actuator, the annular angle θ of the plasma region origination point relative to the y-axis is defined (such as the angle between the line O'A and the y-axis in Fig. 7, here O' is the center of the arc shaped the airfoil trailing edge). In this definition, the annular angle for the original edge of plasma region in this section (Point A) is $\theta = 15°$.

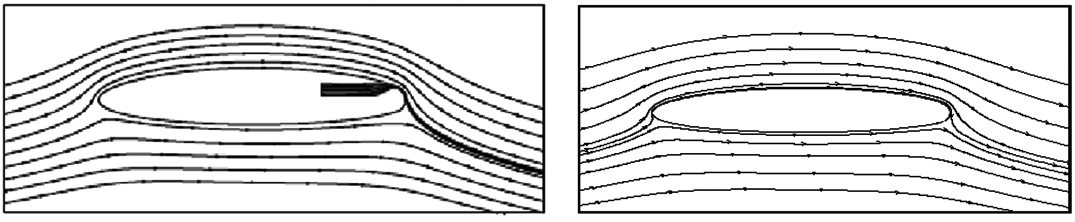

a) FSRM simulated flow field by Chang et al. [31] **b) Present simulation**

Fig. 5 Flowfield of NCCR 1510-7067N airfoil with jet CC ($C_\mu = 0.092$).

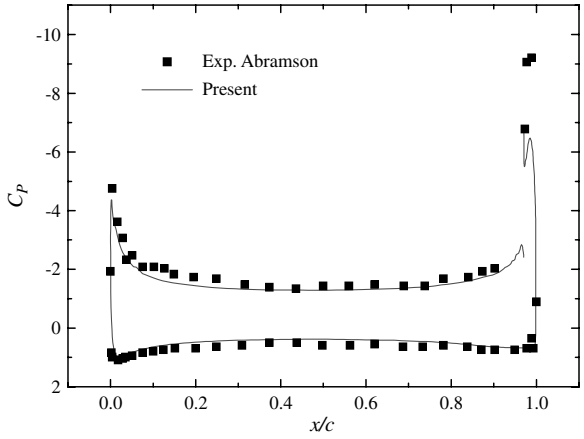

Fig. 6 Pressure distribution of NCCR1510-7067N with jet CC ($C_\mu = 0.092$).

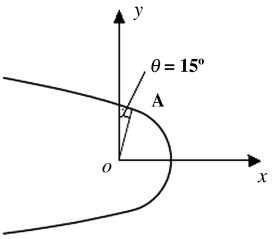

Fig. 7 Sketch of plasma actuator configuration and the definition of coordinate (Point A is the tangential point of the upper surface and the Coanda trailing edge).

Figure 8 presents the aerodynamic characteristics of the airfoil at angle of attack from 0 to 12 ° with/without PCC. It is obvious that plasma actuator has remarkable influence on the aerodynamic forces of airfoil. With the plasma actuator on, the lift coefficient of airfoil dramatically increases. The increment of lift coefficient has just tiny decrease with angle of attack increasing for $0° \leq \alpha \leq 10°$, and a more obvious decrease at 12° (see in Fig. 8a), which dues to the early airfoil leading-edge separation caused by the airfoil circulation increase. The unique advantage for this lift enhancement method is that the lift increment is considerable at low angle of attacks. For example, the lift coefficient of airfoil with PCC increases from 0.086 to 0.904 at zero angle of attack in present simulation, which is almost the maximum lift coefficient of a general airfoil. This feature is very important to improve the aircraft low speed performances, such as decrease the takeoff/landing roll distance or increase the low speed maneuverability [30,47]. With PCC actuated, the lift to drag ratio of airfoil also increases for angle of attack $0° \leq \alpha \leq 12°$, which is presented in Fig. 8b. Especially, the maximum lift to drag ratio increases from 29.69 to 41.17 at angle of attack $\alpha = 4°$, which means it increases by 38.7% compared with that of the cleaning airfoil.

To explain the mechanism for lift enhancement, Fig. 9 gives the flow field around the airfoil for angle of attack $0° \leq \alpha \leq 12°$ with/without PCC to compare, in which the variation of the leading-edge and trailing-edge stagnation points should be pay more attention. Before the plasma actuator is excited, the circulation of airfoil increases with the angle of attack increasing, which induces the leading-edge stagnation point moves downward to the lower surface of airfoil. The boundary layer on upper surface of airfoil separates near the trailing edge, which forms the wake vortex region downstream of airfoil. With PCC, the ambient neutral air is absorbed into the plasma region and forms a high-velocity wall jet compared with the surrounding boundary-layer flow (see in Fig. 10), which attaches to the trailing-edge surface due to Coanda effect. So the boundary layer is energized, resulting in a delay in separation and the downward movement of leading-edge and trailing-edge stagnation points (right column in Fig. 9). This means that the circulation of airfoil is direct controlled by the trailing-edge plasma actuator. The

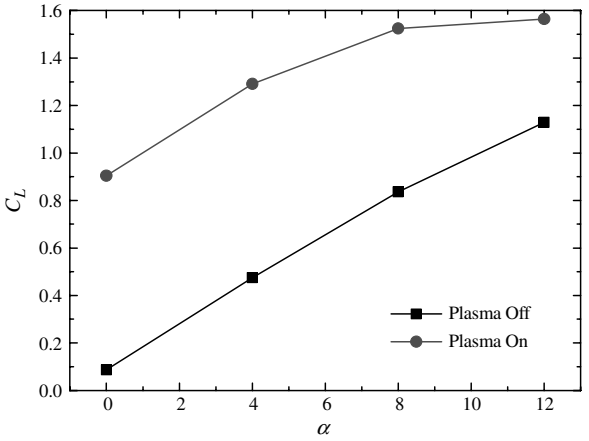

a) Lift coefficient

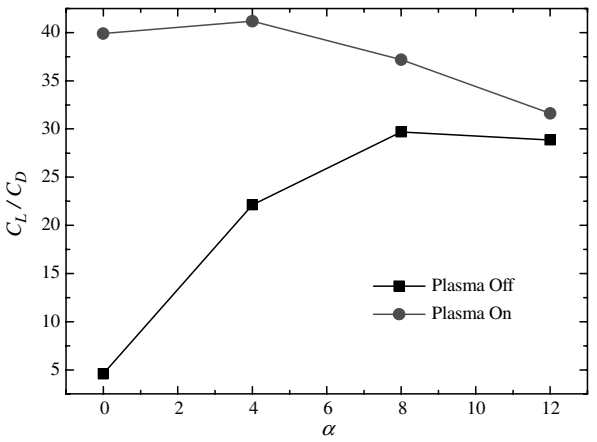

b) Lift coefficient vs. drag coefficient

Fig. 8 Aerodynamic forces variation with angle of attack with PCC on/off.

pressure variation of airfoil induced by PCC is shown in Fig. 11. For the leading-edge and trailing-edge stagnation points migrate to the lower surface of airfoil, the flow accelerates at the leading and trailing edge, which leads to the pressure suction peaks at these two parts. The pressure difference of upper and lower surface of airfoil also increases with PCC, so the lift by integrating the pressure presents remarkable increase as shown in Fig. 8a. Compared with that in jet CC investigations, the flow structure around airfoil, the leading-edge and trailing-edge stagnation points variation, the velocity vector in the boundary near the actuator and the change of pressure distribution induced by PCC are all similar to previous experimental [48,49] and numerical results [31] with jet CC, so it can be concluded that wall jet induced by the plasma actuator can achieve the effect as pneumatic jet, which means can control the circulation of airfoil using Coanda effect.

From previous discussion, it is known that the lift increment decreases a lot at angle of attack $\alpha = 12°$ (as shown in Fig. 8a), which is caused by the different flow characteristics of airfoil at high angle of attack. At low angles of attack, the leading-edge and trailing-edge stagnation points can be moved downward to lower surface with considerable distance with PCC (see in Figs. 9a and 9b), which leads to the pressure suction peaks at the airfoil leading and trailing edge, and subsequent increase of pressure difference between the upper and lower surface of airfoil (see in Figs. 11a and 11b). While at high angle of attack ($\alpha = 12°$), the leading-edge stagnation point is located at the lower surface of airfoil before the plasma actuator is excited, which results in the corresponding pressure suction peak appears at the leading edge. Meanwhile, the upper surface boundary layer separates in advance near the trailing edge at high angle of attack. With these two factors, the variation of the leading-edge and trailing-edge stagnation points at high angle of attack is smaller than

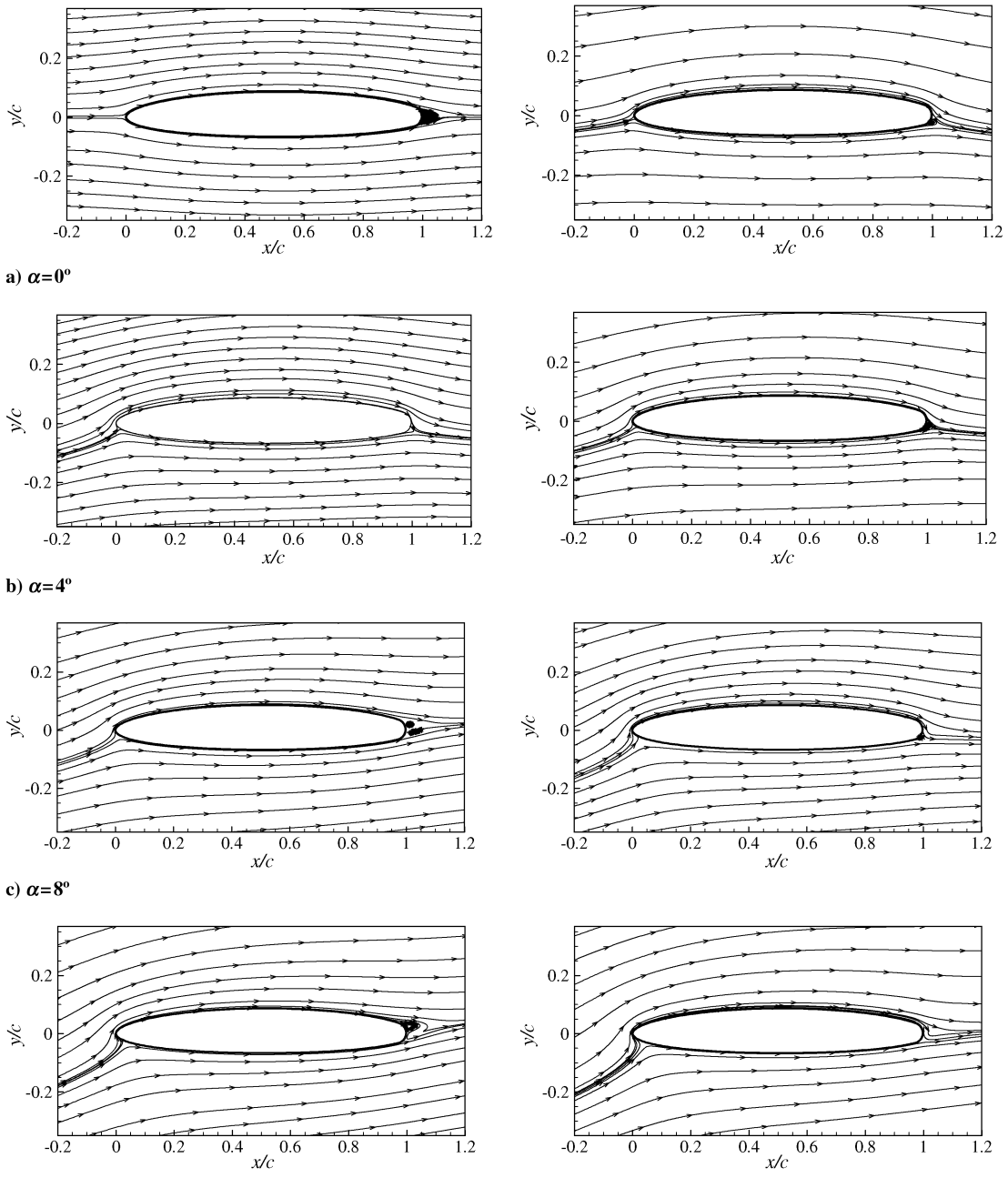

Fig. 9 Flowfield around the airfoil with/without PCC (left: without control, right: with control).

that at low angle of attack (see in Fig. 9d), so the pressure distribution of airfoil with PCC has a little difference to that of original airfoil (see in Fig. 11d). This is the answer to why the lift increment with PCC is small in Fig. 8a at angle of attack $\alpha = 12°$. If the angle of attack further increases close to the original airfoil stall angle, the leading-edge stagnation point will keep on moving downward due to the incoming flow and the PCC effect, which causes the early leading-edge stall. Then the lift drops, and the CC has little effect at this situation [31,32]. This feature also indicates that PCC technique can increase the lift of airfoil only at low angle of attack, similar to that of jet CC. At high angle of attack, the trailing edge is totally merged in the separated wake region, so the flow control devices, especially with steady excitation, have no capability to improve the aerodynamic performance of airfoil. In anther word, since the lift augmentation efficiency of CC is extremely higher than the traditional mechanical lift enhancement devices, so even at low angle of attack, the airfoil with PCC can produce enough lift coefficient for aircraft takeoff/landing at low speed [30,33].

The Coanda blowing jet produced by plasma actuator is driven by body force adding to the fluids in plasma region, which is essentially tangential to the airfoil surface. While the conventional pneumatic CC jet comes from a slot on the airfoil and it must have an incline angle to the airfoil surface, no matter how much. This requires the pneumatic jet should be suppressed by the main outflow to be tangential to the airfoil surface. In this process, the pneumatic jet wastes a portion of energy to resist the main flow. Based on this point, the plasma-induced Coanda blowing jet used in the present study is superior to the conventional pneumatic jet in CC on airfoil.

To compare the efficiency of plasma-induced Coanda blowing jet with conventional pneumatic jet in CC, Fig. 12 gives the lift augmentation of NCCR 1510-7067N airfoil at $\alpha = 0°$ with CC by these two methods. For convenient to compare, the equivalent jet momentum coefficient C_μ of plasma actuator with $Dc = 22.7$ is estimated by integration the tangential velocity profile in boundary layer, here the integration path is normal to the airfoil surface and just

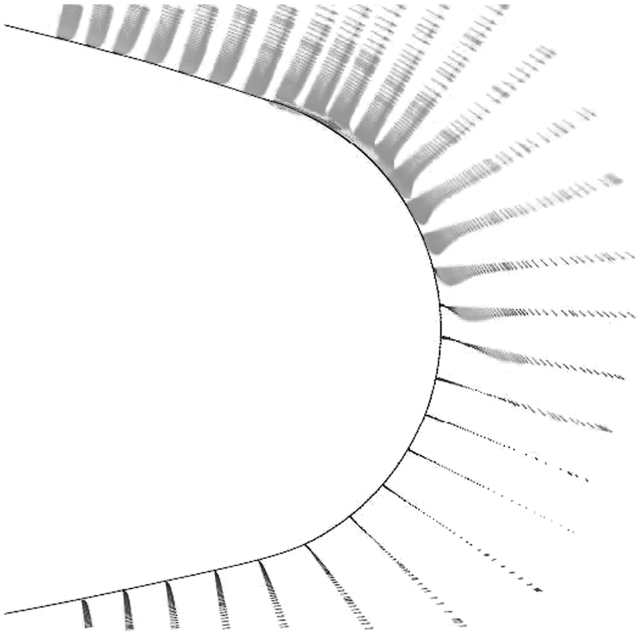

Fig. 10 Velocity vector near the airfoil trailing edge with PCC ($\alpha = 0°$).

at the downstream edge of the plasma region. The formula is as follows:

$$C_\mu = \frac{\int_0^\delta \rho u_\tau^2(n) \cdot n \, \mathrm{d}n}{\frac{1}{2}\rho_\infty U_\infty^2 c} \tag{5}$$

here, $u_\tau(n)$ is the velocity tangential to airfoil surface, δ is the boundary-layer momentum thickness. From the flow field simulated, the integration gives the comparable jet momentum efficient of plasma-induced blowing jet in present study $C_\mu = 0.01$, which is shown as a star symbol in Fig. 12 with the corresponding lift augmentation $\Delta C_L = 0.818$. Compared with the pneumatic blowing jet results in the same figure, it is known that the jet momentum efficient should be $C_\mu = 0.031$ for the convention jet CC to achieve the same lift augmentation as the plasma actuator used in present. According to the lift augmentation efficiency definition ($\Delta C_L/C_\mu$), the lift augmentation efficiency of PCC in present simulation is $\Delta C_L/C_\mu = 81.8$, which is higher enough than the value of 31 for conventional jet CC shown in Fig. 12, and is comparable to the maximum lift augmentation efficiency 80 for conventional jet CC in all published literatures up to now [5,6]. To eliminate the effect of the trailing-edge shape modification, two additional cases of the plasma actuator placed at the same annual angle 30° on the original and modified trailing edge were also simulated. The lift coefficients of airfoil with PCC in these two cases only have little difference. Hence, the effect of the trailing-edge shape modification is negligible in present study.

VI. Effect of Annular Angle of Plasma Actuator

As discussed in introduction, the Coanda blowing jet is essentially required to be tangential to airfoil surface, which makes the blowing jet adhere to the curve wall matching the Coanda effect condition. In jet CC, the slot should be specially designed to let the jet tangential to the airplane surface, which is usually placed at the smooth transient position at the airfoil trailing edge connected with the airfoil upper surface. In this consideration, the location of slot is mainly based on the airfoil geometry, and can not take fully into account the features of boundary-layer separation. Actually, the airfoil jet CC has close relationship with the boundary-layer separation characteristics, especially the separation point location. Hence, it is necessary to investigate the effect of actuation location on the lift enhancement of airfoil with CC and pursue the optimum solution.

Because of the advantage of plasma actuator flexibility [14], the PCC device can be placed at any location on airfoil trailing edge and

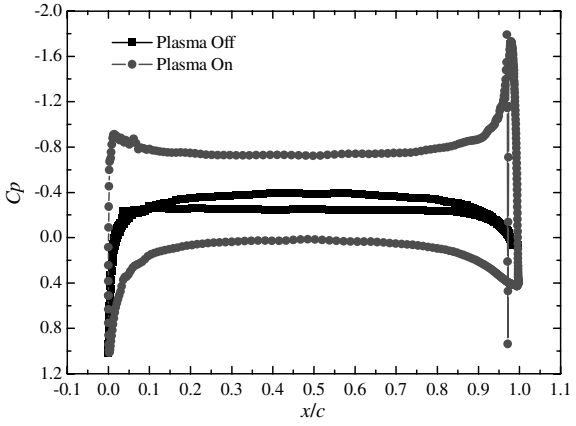

a) α=0°

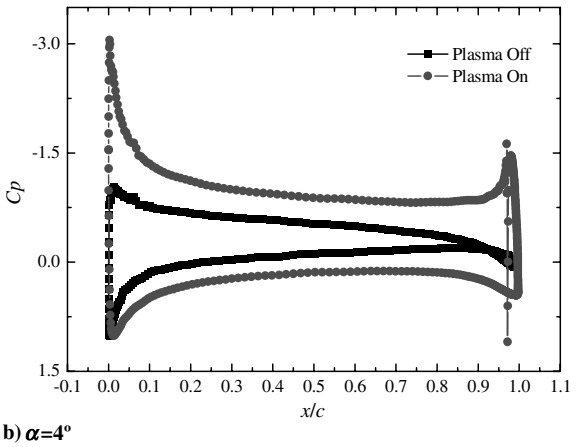

b) α=4°

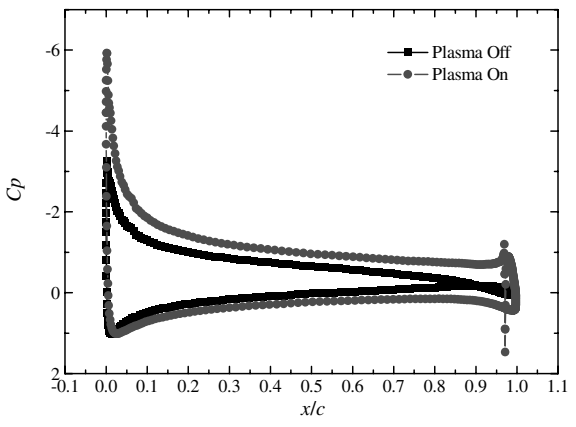

c) α=8°

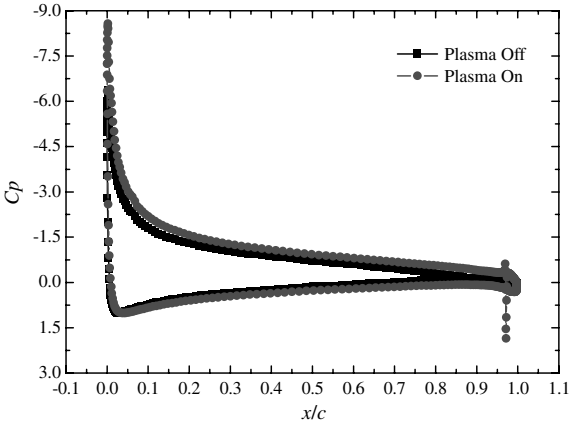

d) α=12°

Fig. 11 Pressure distribution on the airfoil with/without PCC.

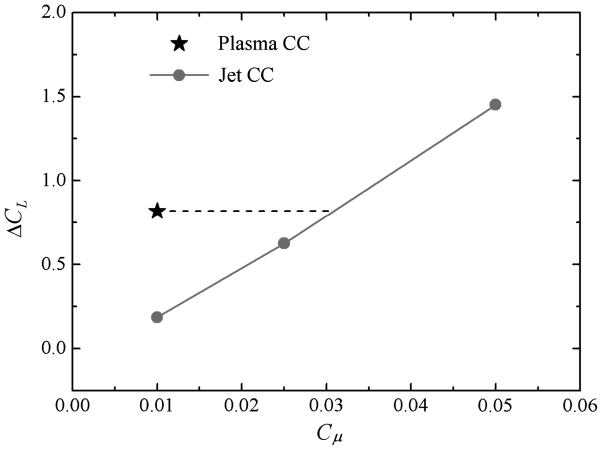

Fig. 12 Lift augment efficiency for NCCR 1510-7067N airfoil at $\alpha = 0°$ of PCC compared with jet CC.

produces Coanda blowing jet tangential to the airfoil surface. The airfoil geometry is no longer the limitation for actuator configuration, and the physical mechanism for separation/CC can be paid more attention in study. In this section, the annular angle θ of the plasma region is changed to investigate the effect of plasma actuator location on PCC. There are seven locations for the plasma actuator in simulation. The first one is the baseline case at point A shown in Fig. 7 discussed in last section, the other six locations has an annular angle increment $\Delta\theta = 15°$ one by one. The detail location and annular angle value can be seen in Table 1.

With the variation of the annular angle, the lift coefficient and its increment at angle of attack from 0 to 12° are presented in Fig. 13. It is obvious that the lift of airfoil with PCC in all cases increases compared with that of cleaning airfoil. With annular angle $\theta \leq 60°$, the lift augmentation of airfoil with PCC decreases with angle of attack increasing, which is similar to the results shown in last section. This trend is clearly presented in Fig. 13b with lift coefficient increment. While for annular angle $\theta \geq 75°$, the annular angle has little effect on the lift argumentation of airfoil by PCC (as shown in Fig. 13b). The lift coefficient increment has almost the same value in the whole range of attack angle. Another interesting phenomenon is that the lift increment has large variation at zero angle of attack with different annular angle. It is shown that the lift coefficient increment is only $\Delta C_L = 0.245$ at $\theta = 75°$, but increases to $\Delta C_L = 1.349$ at $\theta = 45°$. This means that the lift performance of airfoil at zero angle of attack with PCC can be adjusted by changing the plasma actuator location. It is not like the traditional airfoil, whose lift coefficient is absolutely depending on the angle of attack. This characteristic is very important for the STOL and VTOL aircraft design [3]. The lift augmentation efficiency after the location optimization reaches to $\Delta C_L/C_\mu = 134.86$ at zero angle of attack with annular angle $\theta = 45°$, which is much higher than the maximum lift augmentation efficiency 80 for conventional jet CC in previous discussion. So PCC is not only easy to integrate into existing aircraft, but also has superior lift augmentation efficiency compared with conventional jet CC.

To directly show the lift variation of PPC airfoil with annular angle, Fig. 14 redraws the results in Fig. 13b in the way of the lift coefficient increment vs annular angle at different angles of attack.

Table 1 Annular angles of plasma actuator in simulation

Location	Annular angle θ
A	15°
B	30°
C	45°
D	60°
E	75°
F	90°
G	105°

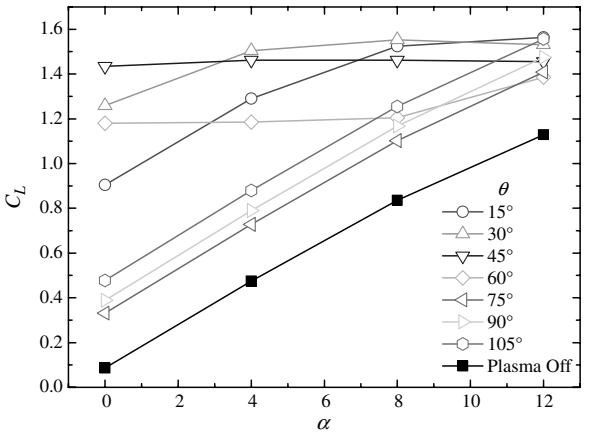

a) Lift coefficient

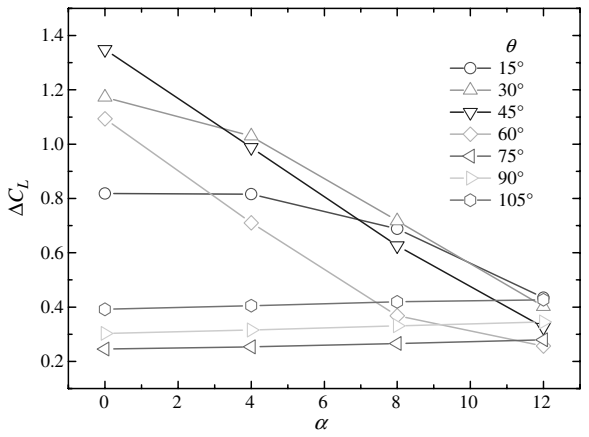

b) Lift coefficient increment

Fig. 13 Lift coefficient and lift increment of airfoil with PCC at different locations varies with angle of attack.

The trailing edge can be divided to two parts by different variation trends of lift increment with annular angle. One is the region for $\theta \leq 60°$, in which the annular angle has significant influence on the lift augmentation effect of PCC. While in the other region for $\theta \geq 75°$, the annular angle has negligible effect compared with that at low annular angle. This feature of aerodynamic force is associated with the flow structure changes as shown in Fig. 15. As annular angle $\theta \leq 60°$ (Figs. 15a–15d), the separated wake region downstream of airfoil trailing edge (left of Fig. 9a) disappears with PCC. The separated shear layer reattaches to the airfoil surface induced by the plasma actuator, and the trailing-edge detachment point is moved aft to the lower surface of airfoil. Meanwhile, the leading-edge stagnation point is also pushed downward to the lower surface of airfoil. The flow on the upper surface of airfoil wraps the leading and trailing edge, which leads to the suction peaks at this two point for flow acceleration (see in Fig. 16). The pressure difference between the upper and lower surface of airfoil increases, so the integrated lift of airfoil is enhanced by PCC. In the other region ($\theta \geq 75°$, Figs. 15e and 15f), the plasma actuator is totally merged in the separated wake of airfoil. It is so far from the location of plasma actuator to the airfoil upper surface boundary-layer separation point, and the plasma actuator has no enough power to suck the separated shear layer back to the airfoil surface again. So there is also a separated wake region downstream of airfoil with PCC in this situation. At the same time, the divergence of the incoming flow to the airfoil chord for $\theta \geq 75°$ is much smaller than that for $\theta \leq 60°$ (see in Fig. 15), and the leading-edge stagnation point for the former is also not pushed downward enough as that in latter cases. The failure of plasma actuator to make the movement of leading-edge and trailing-edge stagnation points results in the disappear of two suction peak in cases for $\theta \geq 75°$, and the pressure difference between the upper and lower surface of airfoil

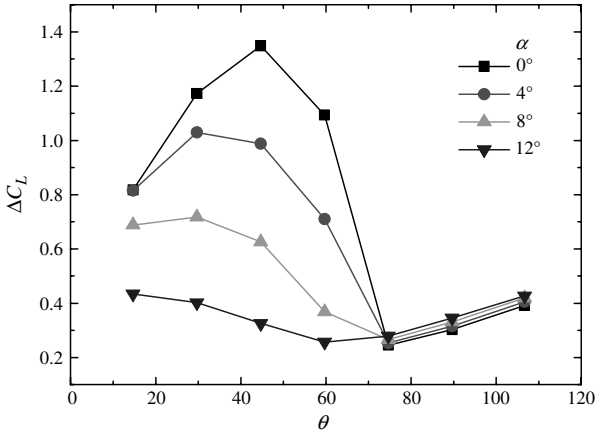

Fig. 14 Lift coefficient increment vs annular angle at different angle of attack.

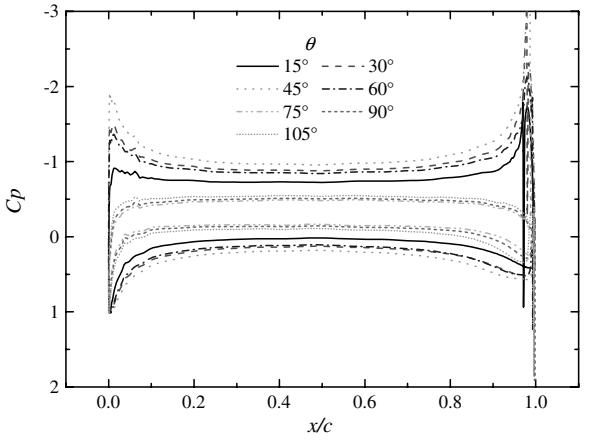

Fig. 16 Pressure distribution on airfoil with PCC at different annular angle ($\alpha = 0°$).

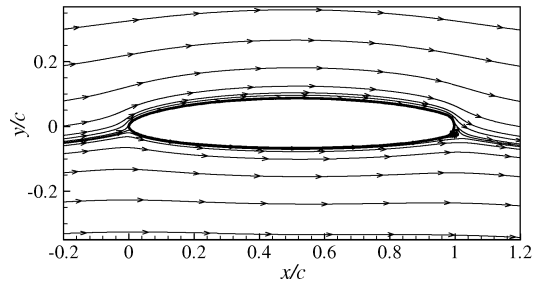

a) θ=15°

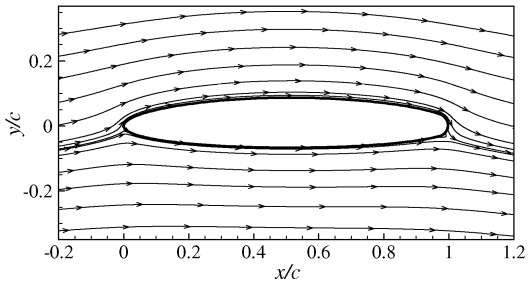

b) θ=30°

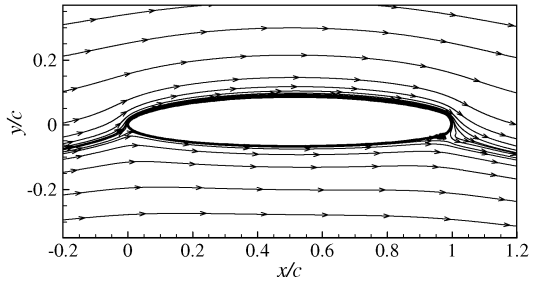

c) θ=45°

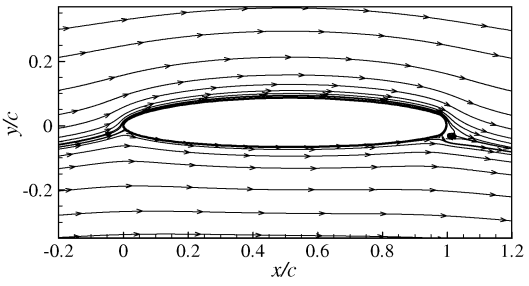

d) θ=60°

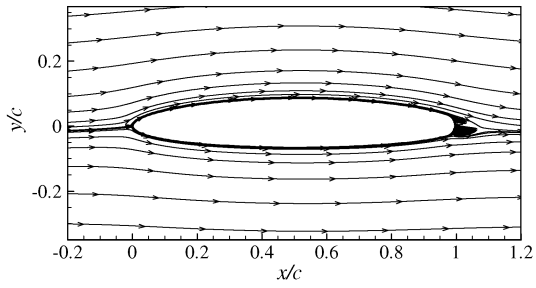

e) θ=75°

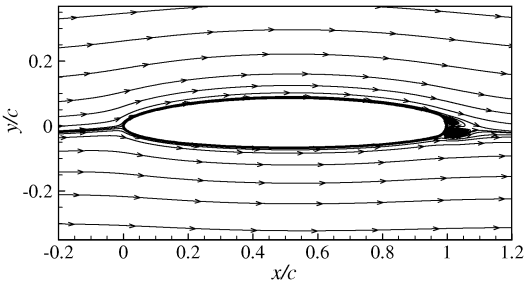

f) θ=90°

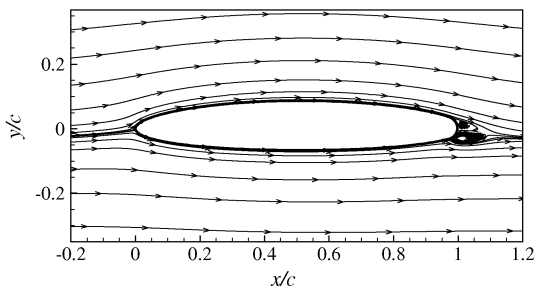

g) θ=105°

Fig. 15 Flow streamline around the airfoil with PCC at different annular angle ($\alpha = 0°$).

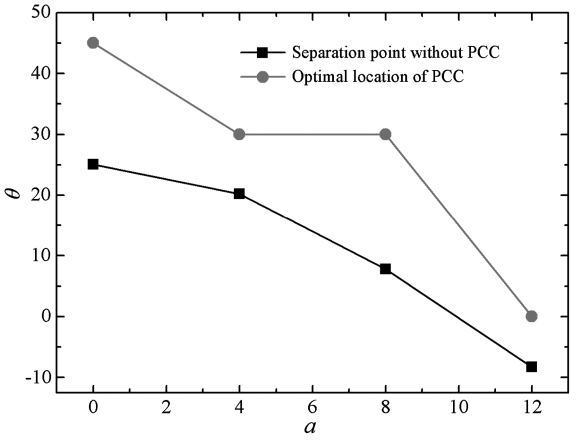

Fig. 17 Optimal locations of PCC and locations of separation point without PCC.

has no change for different annular angle (as shown in Fig. 16). This causes the life increment does not vary with the annular angle $\theta \geq 75°$ in Fig. 14.

At zero angle of attack, in the region ($\theta \leq 60°$), where the annular angle has distinct influence on lift augmentation efficiency of PCC, the lift increment of airfoil with PCC initially increases with annular angle, and reaches the maximum value at $\theta = 45°$ following with a sudden drop at rest angles of attack. While at angle of attack $\alpha = 4$ and 8°, the annular angle, at which the lift of airfoil with PCC has maximum value, changes to $\theta = 30°$. At angle of attack $\alpha = 12°$, the annular angle of plasma actuator with optimum control effect shifts advanced to the first location of plasma actuator $\theta = 15°$, then the lift decreases monotonously with the annular angle increasing. The variation of optimum annular angle at different angle of attack is caused by the boundary-layer separation point movement, because the efficiency for PCC depends on the relative distance between the plasma actuator and the upper surface boundary-layer separation point of airfoil. The optimum location of plasma actuator in PCC is

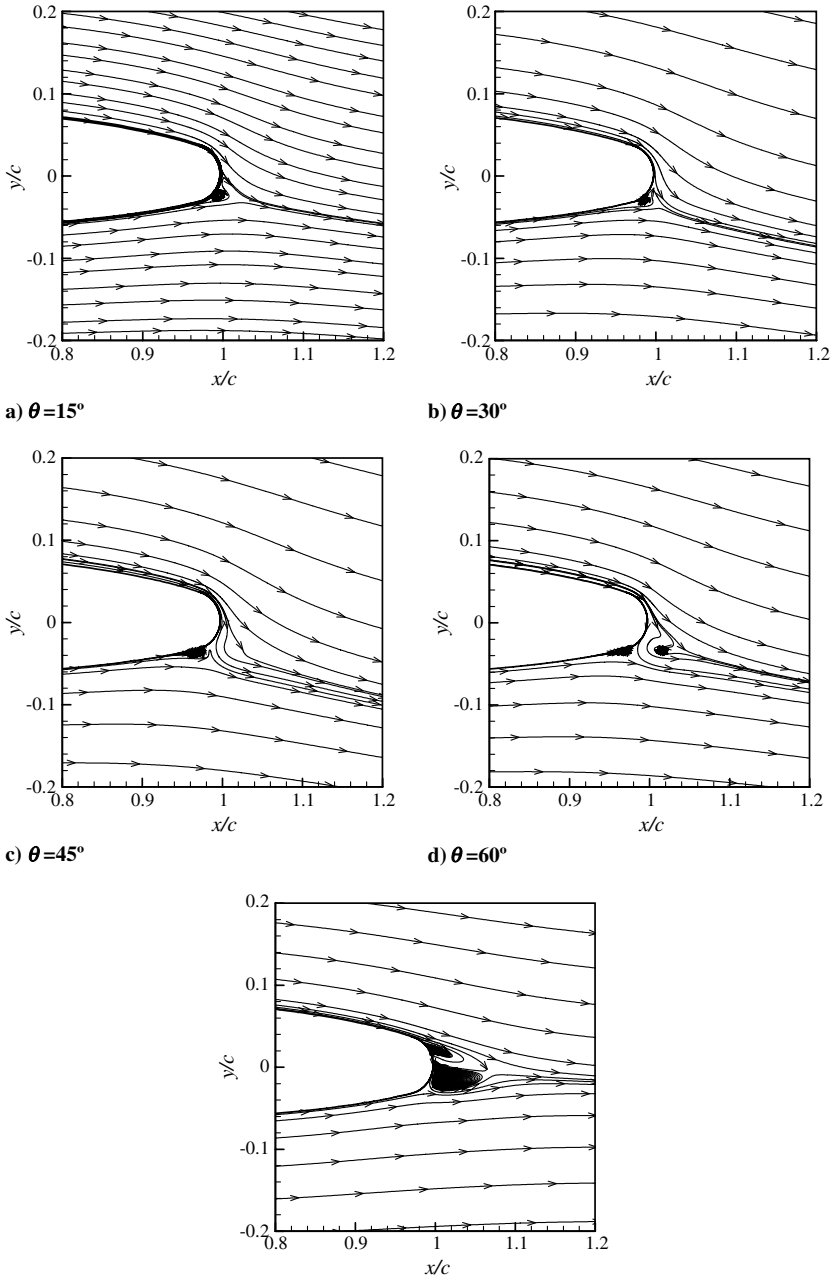

Fig. 18 Flow streamlines near the airfoil trailing edge with PCC at different annular angle ($\alpha = 0°$).

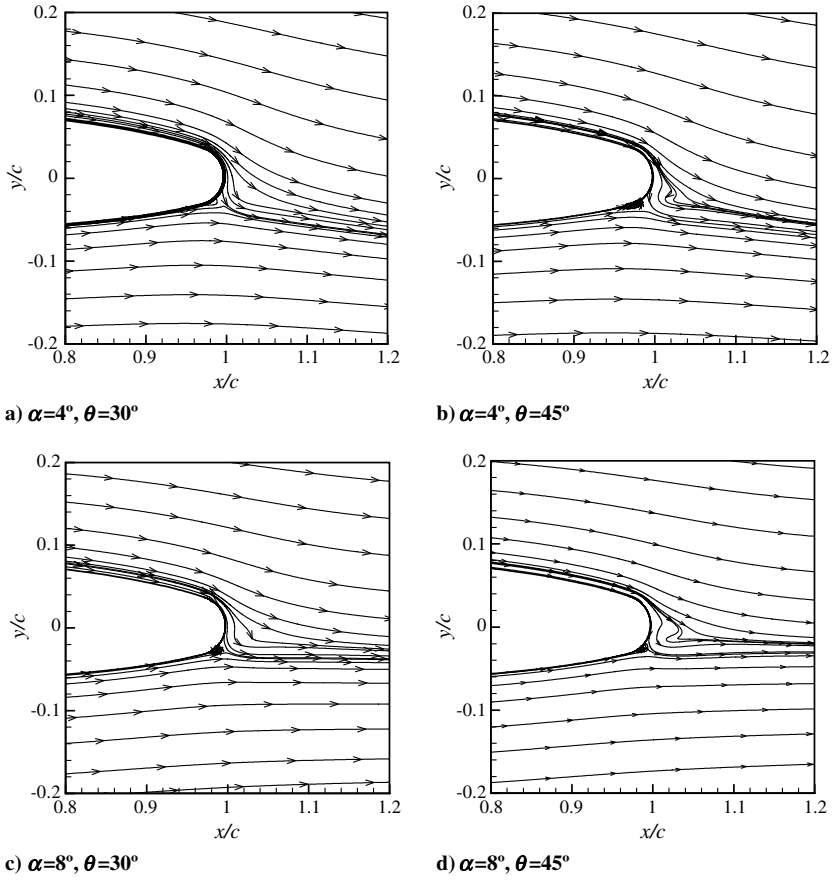

a) α=4°, θ=30° b) α=4°, θ=45°

c) α=8°, θ=30° d) α=8°, θ=45°

Fig. 19 Flow streamlines near the airfoil trailing edge as PCC fails.

downstream of the boundary-layer separation point with a proper distance, where the plasma actuator suction effect has visible influence on the upstream separated shear layer in vicinity and makes it reattach to the airfoil surface, then delays the separation with the wall jet energizing the downstream boundary layer. At the round trailing edge, this blowing jet with high-velocity pushes the trailing-edge detachment point aft to the airfoil lower surface by Coanda effect, and obtains the best efficiency for PCC. This mechanism is the same as that for plasma actuator in separation control, for the unique features of plasma actuator, suction the upstream low speed fluids and acceleration the downstream boundary layer [16,50]. As that in separation flow control, the proper distance of plasma actuator downstream of the separation point in PCC is also affected by the Reynolds number and the relative strength of plasma actuator. For the location far upstream of the boundary separation point or totally merged in the separated wake region, the plasma actuator can not control the circulation of airfoil with the best efficiency.

For the close relationship between the optimum annular angle and the boundary separation point, the optimum annular angle decreases with the angle of attack increasing, for the upper surface boundary-layer separation point of airfoil is advanced with angle of attack increasing (see left column in Fig. 9). The exact airfoil boundary-layer separation angles and the optimum locations of plasma actuator are presented in Fig. 17. The line of the optimal locations of plasma actuator is not smooth for the coarse sample point with an annular angle increment $\Delta\theta = 15°$, but the annular angle of optimum plasma actuator location decreases with angle of attack, followed with the variation of boundary separation point in the same trend. For example, the optimum annular angle changes from $\theta = 45°$ at $\alpha = 0°$ to $\theta = 15°$ at $\alpha = 12°$. The optimum location of plasma actuator in PCC varies from 10 to 20° downstream of the boundary-layer separation point in present study.

At zero angle of attack, the boundary-layer separation point is pushed to at the middle point of the trailing edge by PCC at annular angle $\theta = 15°$ (see in Fig. 18a), then it keeps on moving aft to the lower surface of airfoil with annular angle increasing until $\theta = 45°$ (see in Figs. 18b and 18c). At annular angle $\theta = 45°$, the suction peaks at leading and trailing edges of airfoil have maximum value accompanying with the maximum pressure difference between the upper and lower surface of airfoil (see in Fig. 16), i.e., $Cp < -3$ at the trailing edge, and the integrated lift coefficient has the maximum value, too (seen in Fig. 14). When the plasma actuator is shifted to annular angle $\theta = 60°$ (see in Fig. 18d), the effect of PCC on airfoil starts to decrease, and the corresponding pressure distribution on the upper and lower surface of airfoil has smaller difference compared with that at $\theta = 45°$. While the plasma actuator is totally merged in the separated wake region of airfoil at $\theta = 75 \sim 105°$ (see in Fig. 18e, just presents the flow field near airfoil trailing edge at $\theta = 75°$ as representative), the plasma actuator has no enough power to suck the separated shear layer back to the airfoil surface again, and a large separated vortex wake appears downstream of the airfoil trailing edge, so the lift increment has a sudden drop in the transient region and has almost the same value at $\theta > 75°$ (see in Fig. 14). At other angle of attacks, i.e. $\alpha = 4$ and 8°, when the annular angle increases right over the optimum value, the lift increment obviously decreases, but the location of trailing-edge detachment point has no variation. The only way to decide whether it is the optimum annular angle from the flow field or not is to see flow pattern in the separated wake region downstream of airfoil trailing edge (see in Fig. 19). If the separation point has no variation with annular angle increasing, but the separated vortex appears in the airfoil downstream wake region, it can be considered that the plasma actuator is placed at right over the optimum annular angle to control the circulation of airfoil. After that, the von Kármán vortex street appears in the wake region and the PCC device is failure to enhance the lift of airfoil (see in Figs. 15e–15g).

VII. Conclusions

A novel PCC method is proposed by using the plasma actuator induced wall jet as Coanda blowing jet. By fabricated with flexible

materials for printed circuit board, the plasma actuator can be placed at any complex sharp surfaces of the airplane. So the PCC device overcomes the disadvantage of conventional jet PCC system for air source supply, and can be easily integrated to the existing aircraft with little modification.

The effect of PCC on the aerodynamic characteristics improvement of NCCR 1510-7067N elliptic airfoil is demonstrated by solving the Reynolds-Averaged Navier–Stokes equations. The plasma actuator is modeled with a phenomenological model. The simulated results indicate that PCC can dramatically increase the lift coefficient of airfoil at low angle of attack. As the plasma-induced wall jet is essentially tangential to the airfoil surface, the lift augmentation efficiency after the location optimization reaches to $\Delta C_L/C_\mu = 134.86$, which is much higher than the maximum lift augmentation efficiency 80 for conventional jet CC. So the efficiency of PCC for lift augmentation is superior to that of conventional jet CC.

The optimal location for the plasma actuator in PCC is downstream of the boundary-layer separation point with proper distance, where the plasma actuator makes the separated shear layer reattach to the airfoil surface and delays the separation by Coanda effect. Right over this annular angle, the boundary-layer separation point has no variation with annular angle increasing, but the separated vortex appears in the airfoil downstream wake region. When the plasma actuator is totally merged in the separated wake of airfoil, it has no enough power to suck the separated shear layer back to the airfoil surface again. At this situation, the plasma actuator fails to control the circulation of airfoil, and the lift of airfoil does not vary with plasma actuator location and the angle of attack.

Acknowledgments

The present research was supported by the National Natural Science Foundation of China under grant no. 10872021 and the Specialized Research Fund for the Doctoral Program of High Education of China under grant no. 200800061040. The first author would like to thank to Wei Shyy from the University of Michigan for the suggestions in revising the manuscript.

References

[1] Coanda H., "Device for Deflecting a Stream of Elastic Fluid Projected into an Elastic Fluid," U.S. Patent No. 2,052,869, 1936.

[2] Liu, Y., "Numerical Simulation of the Aerodynamic Characteristics of Circulation Control Wing Sections," Ph.D. Dissertation, School of Aerospace Engineering, Georgia Institute of Technology, Atlanta, GA, 2003.

[3] Englar, R. J., "Overview of Circulation Control Pneumatic Aerodynamics: Blown Force and Moment Augmentation and Modification as Applied Primarily to Fixed-Wing Aircraft," *Proceedings of the 2004 NASA/ONR Circulation Control Workshop*, Part 1, NASA/Office of Naval Research, pp. 37–99.

[4] Cheeseman, I. C., "Circulation Control and its Application to Stopped Rotor Aircraft," AIAA Paper 67-747, Oct. 1967.

[5] Englar, R. J., and Williams, R. M., "Test Techniques for High-Lift, Two-Dimensional Airfoils with Boundary Layer and Circulation Control for Application to Rotary Wing Aircraft," *Canadian Aeronautics and Space Journal*, Vol. 19, No. 3, March 1973, pp. 93–108.

[6] Englar, R. J., Niebur, C. S., and Gregory, S. D., "Pneumatic Lift and Control Surface Technology for High Speed Civil Transport Configurations," *Journal of Aircraft*, Vol. 36 No. 2, 1999, pp. 332–339. doi:10.2514/2.2454

[7] Englar, R. J., and Huson, G. G., "Development of Advanced Circulation Control Wing High Lift Airfoils," *Journal of Aircraft*, Vol. 21, No. 7, 1984, pp. 476–483. doi:10.2514/3.44996

[8] Englar, R. J., "Low-Speed Aerodynamic Characteristics of a Small Fixed-Trailing-Edge Circulation Control Wing Configuration Fitted to a Supercritical Airfoil," DTNSRDC Rept. ASED-81/08, March 1981.

[9] Englar, R. J., Marilyn, J. S., Sean, M. K., and Richard, C. R., "Development of Circulation Control Technology for Application to Advanced Subsonic Transport Aircraft, Part 1: Airfoil Development," *Journal of Aircraft*, Vol. 31, No. 5, 1994, pp. 1160–1168. doi:10.2514/3.56907

[10] Englar, R. J., Marilyn, J. S., Sean, M. K., and Richard, C. R., "Development of Circulation Control Technology for Application to Advanced Subsonic Transport Aircraft, Part 2: Transport Application," *Journal of Aircraft*, Vol. 31, No. 5, 1994, pp. 1169–1171. doi:10.2514/3.46627

[11] Englar, R. J., Niebur, J. S., and Gregory, S. D., "Pneumatic Lift and Control Surface Technology for High Speed Civil Transports," *Journal of Aircraft*, Vol. 36, No. 2, 1999, pp. 332–339. doi:10.2514/2.2454

[12] John, L. L., "Why Have Only Two Circulation-Controlled STOL Aircraft Been Built and Flown in Years 1974–2004," *Proceedings of the 2004 NASA/ONR Circulation Control Workshop*, Part 2, NASA/Office of Naval Research, pp. 603–622.

[13] Corke, T. C., Post, M. L., and Orlov, D. M., "SDBD Plasma Enhanced Aerodynamics: Concepts, Optimization and Applications," *Progress in Aerospace Sciences*, Vol. 43, Nos. 7–8, 2007, pp. 193–217. doi:10.1016/j.paerosci.2007.06.001

[14] Greenblatt, D., Kastantin, Y., Nayeri, C. N., and Paschereit, C. O., "Delta Wing Flow Control Using Dielectric Barrier Discharge Actuators," *AIAA Journal*, Vol. 46 No. 6, 2008, pp. 1554–1560. doi:10.2514/1.33808

[15] Roth, J. R., Tsai, P. P., and Liu, C., U.S. Patent No. 5387842, 1995.

[16] Moreau, E., "Airflow Control by Nonthermal Plasma Actuators," *Journal of Physics D: Applied Physics*, Vol. 40, No. 3, 2007, pp. 605–636. doi:10.1088/0022-3727/40/3/S01

[17] Shyy, W., Jayaraman, B., and Andersson, A., "Modeling of Glow-Discharge Induced Fluid Dynamics," *Journal of Applied Physics*, Vol. 92, No. 11, 2002, pp. 6434–6443. doi:10.1063/1.1515103

[18] Jayaraman, B., and Shyy, W., "Modeling of Dielectric Barrier Discharge-Induced Fluid Dynamics and Heat Transfer," *Progress in Aerospace Sciences*, Vol. 44, No. 3, 2008, pp. 139–191. doi:10.1016/j.paerosci.2007.10.004

[19] Jayaraman, B., Lian, Y., and Shyy, W., "Low-Reynolds Number Flow Control Using Dielectric Barrier Discharge Actuators," 37th AIAA Fluid Dynamics Conference and Exhibit, AIAA Paper 2007-3974, Miami, FL, 25–28 June 2007.

[20] Gaitonde, D. V., Visbal, M. R., and Roy S., "Control of Flow past a Wing Section with Plasma-Based Body Forces," AIAA Paper 2005-5302, 2005.

[21] Jayaraman, B., and Shyy, W., "Flow Control and Thermal Management Using Dielectric Glow Discharge Concepts," AIAA Paper 2003-3712, 2003.

[22] Orlov, D. M., "Modeling and Experiment of Leading Edge Separation Control Using SDBD Plasma Actuators," AIAA Paper 2007-0877, 2007.

[23] He, C., and Corke, T. C., "Numerical and Experimental Analysis of Plasma Flow Control over a Hump Model," 45th AIAA Aerospace Sciences Meeting and Exhibit, AIAA Paper 2007-0935, Reno, NV, 8–11 Jan. 2007.

[24] Visbal, M. R., and Gaitonde, D. V., "Control of Transitional and Turbulent Flows Using Plasma-Based Actuators," AIAA Paper 2006-3230, 2006.

[25] Rizzetta, D. P., and Visbal, M. R., "Numerical Investigation of Plasma-Based Flow Control for a Transitional Highly-Loaded Low-Pressure Turbine," AIAA Paper 2007-0938, 2007.

[26] Vo, H. D., "Control of Rotating Stall in Axial Compressors Using Plasma Actuators," AIAA Paper 2007-3845, 2007.

[27] Lemire, S., Vo, H. D., and Benner, M. W., "Performance Improvement of Axial Compressors and Fans with Plasma Actuation," *International Journal of Rotating Machinery*, Vol. 2009, 2009.

[28] Fu, X., Li, Y., Li, B., and Kwok, D. Y., "Drag Force Reduction on an Airfoil via Glow Discharge Plasma-Based Control," *European Physical Journal Special Topics*, Vol. 171, No. 1, 2009, pp. 195–204. doi:10.1140/epjst/e2009-01029-3

[29] Gaitonde, D. V., Visbal, M. R., and Roy S., "A Coupled Approach for Plasma-Based Flow Control Simulations of Wing Sections," AIAA Paper 2006-1205, 2006.

[30] Liu, Y., Sankar, L., Englar, R., and Ahuja K., "Numerical Simulations of the Steady and Unsteady Aerodynamic Characteristics of a Circulation Control Wing Airfoil," 39th AIAA Aerospace Sciences Meeting, Reno, NV, AIAA Paper 2001-0704, 2001.

[31] Chang, P. A., Slomski J. F., Marino T., Ebert, M. P., and Abramson, J., "Full Reynolds Stress Modeling of Circulation Control Airfoils," *Proceedings of the 2004 NASA/ONR Circulation Control Workshop (C)*, NASA, Hampton, VA, 2005, pp. 37–75.

[32] Slomski, J. F., Gorski J. J., Miller, R. W., and Marino T. A., "Numerical Simulation of Circulation Control Airfoils as Affected by Turbulence

Models," AIAA Paper 2002-0851, 2002.
[33] Paterson, E. G., and Baker, W. J., "Simulation of Steady Circulation Control for Marine-Vehicle Control Surfaces," AIAA Paper 2004-0748, Jan. 2004.
[34] Swanson, R. C., Rumsey, C. L., and Anders, S. G., "Progress Towards Computational Method for Circulation Control Airfoils," AIAA Paper 2005-0089, Jan. 2005.
[35] Salem, A. A., and Ragab, S. A., "RANS Simulation of Circulation Control on a Circular Planform Wing," AIAA Paper 2008-4326, 2008.
[36] Swanson, R. C., and Rumsey, C. L., "Numerical Issues for Circulation Control Calculations," AIAA Paper 2006-3008, 2006.
[37] Abramson, J., "Two-Dimensional Subsonic Wind Tunnel Evaluation of Two Related Cambered 15-Percent-Thick Circulation Control Airfoils," DTNSRDC TR, 1977.
[38] Jones, G. S., and Joslin, R. D., 2004 NASA/Office of Naval Research Circulation Control Workshop, NASA Rept. CP-2005-213509, June 2005.
[39] Messam, N. A., "Prediction of Circulation Control Performance Characteristics for Super STOL and STOL Applications," Ph.D. Dissertation, School of Aerospace Engineering, Georgia Institute of Technology, Atlanta, GA, 2006.
[40] Roth, J. R., Sherman, D. M., and Wilkinson S. P., "Boundary Layer Flow Control with a One Atmosphere Uniform Glow Discharge," AIAA 36th Aerospace Sciences Meeting and Exhibit, AIAA Paper 98-0328, Reno, NV, 12–15 Jan. 1998.
[41] Roth, J. R., Sherman, D. M., and Wilkinson, S. P., "Electro Hydrodynamic Flow Control with a Glow Discharge Surface Plasma," *AIAA Journal*, Vol. 38, No. 7, 2000, pp. 1166–1172. doi:10.2514/2.1110
[42] Zhang, P. F., Liu, A. B., and Wang, J. J., "Aerodynamic Modification of NACA0012 Airfoil by Trailing Edge Plasma Gurney Flap," *AIAA Journal*, Vol. 47, No. 10, 2009, pp. 2467–2474. doi:10.2514/1.43379
[43] Jayaraman, B., Cho, Y. C., and Shyy, W., "Modeling of Dielectric Barrier Discharge Plasma Actuator," AIAA Paper 2007-4531, 2007.
[44] Van Dyken, R., McLaughlin, T. E., and Enloe, C. L., "Parametric Investigations of a Single Dielectric Barrier Plasma Actuator," AIAA Paper 2004-0946, 2004.
[45] Grundmann, S., Klumpp, S., and Tropea, C., "Experimental and Numerical Investigations of Boundary-Layer Influence Using Plasma-Actuators," *Active Flow Control*, edited by King, R., Springer–Verlag, Berlin, 2007, pp. 56–68.
[46] Corke, T. C., and Matlis, E., "Phased Plasma Arrays for Unsteady Flow Control," AIAA Paper 2000-2323, 2000.
[47] Liu, Y., Sankar, L. N., Englar, R. J., Ahuja, K. K., and Gaeta, R., "Computational Evaluation of the Steady and Pulsed Jet Effects on the Performance of a Circulation Control Wing Section," AIAA Paper 2004-56.
[48] Wetzel, D., Griffin, J., Liu, F., and Cattafestaz, L., "An Experimental Study of Circulation Control on an Elliptic Airfoil," AIAA Paper 2009-4280.
[49] Jones, G. S., Yao, C., and Allan, B. G., "Experimental Investigation of a 2D Supercritical Circulation-Control Airfoil Using Particle Image Velocimetry," AIAA Paper 2006-3009.
[50] Okita1 Y., Jukes, T. N., Choi, K. S., and Nakamura, K., "Flow Reattachment over an Airfoil Using Surface Plasma Actuator," AIAA Paper 2008-4203.

M. Glauser
Associate Editor